Chemical Engineering Journal 155 (2009) 466–473

Contents lists available at ScienceDirect

Chemical Engineering Journal

journal homepage: www.elsevier.com/locate/cej

Preparation, characterization and activity evaluation of p–n junction photocatalyst p-$CaFe_2O_4$/n-ZnO

Chen Shifu*, Zhao Wei, Liu Wei, Zhang Huaye, Yu Xiaoling

Department of Chemistry, Huaibei Coal Normal College, Dongshan 100, Anhui, Huaibei, 235000, People's Republic of China

ARTICLE INFO

Article history:
Received 26 March 2009
Received in revised form 12 June 2009
Accepted 4 July 2009

Keywords:
p-$CaFe_2O_4$/n-ZnO
p–n junction
Photocatalyst
Ball milling
Characterization

ABSTRACT

p–n junction photocatalyst p-$CaFe_2O_4$/n-ZnO was prepared by ball milling of ZnO in H_2O doped with p-type $CaFe_2O_4$. The structural and optical properties of the p–n junction photocatalyst p-$CaFe_2O_4$/n-ZnO were characterized by X-ray powder diffraction (XRD), scanning electron microscopy (SEM), transmission electron microscopy (TEM), UV–vis diffuse reflection spectrum (DRS) and fluorescence emission spectra. The photocatalytic activity of the photocatalyst was evaluated by photocatalytic degradation of methylene blue (MB). The results showed that the photocatalytic activity of the p-$CaFe_2O_4$/n-ZnO was higher than that of ZnO. When the amounts of doped p-$CaFe_2O_4$ were 0.0 wt.% and 1.0 wt.%, the photocatalytic degradation efficiencies were 50.1 and 73.4%, respectively. Effect of ball milling time on the photocatalytic activity of the photocatalyst was also investigated. The mechanisms of influence on the photocatalytic activity were also discussed by the p–n junction principle.

1. Introduction

Owing to their high activities, lower costs, and environment-friendly features, TiO_2 and ZnO have been widely used as photocatalysts [1–7]. Recently, a number of studies related to the syntheses of TiO_2 and ZnO photocatalysts have been reported, including nanoparticles [8–14], nanorods [15,16], nanocrystals [17–19], nanotubes [20], mesoporous TiO_2, and composite membrane. However, the photocatalytic activities of ZnO and TiO_2 are limited to irradiation wavelengths in the UV region because they have wide band-gaps and can only absorb UV light. Some problems still remain to be solved in its application, such as the fast recombination of photogenerated electron–hole pairs. Therefore, improving photocatalytic activity by modification has become a hot topic among researchers in recent years [21–25]. One approach is to dope transition metals into ZnO (or TiO_2), and the other is to form coupled photocatalysts [26–31].

In the past decade, the photocatalytic activity of TiO_2 or ZnO coupled with metal oxides, like SiO_2 [32,33], SnO_2 [34–36], WO_3 [37,38], Fe_2O_3 [39] and some rare earth oxides was investigated [40], for the purpose of improving the photocatalytic activity of TiO_2 or ZnO. The results showed that coupled semiconductor photocatalysts are a novel approach to achieve a more efficient charge separation, an increased lifetime of the charge carriers, and an enhanced interfacial charge transfer to adsorbed substrates. At the same time, their physical and optical properties are greatly modified [37]. Recently, coupled photocatalyst has been studied extensively [41–44], the results showed that the photocatalytic activity of coupled photocatalyst is higher than that of the single one.

It is known that, in photocatalytic systems, p–n junction or heterodiode is also an interesting structure because the formation of p–n junction photocatalyst could lead to an efficient separation of photoexcited electron–hole [45–52]. Recently, Lee and co-workers reported that a p–n junction photocatalyst p-$CaFe_2O_4$/n-$PbBi_2Nb_{1.9}W_{0.1}O_9$ had a very high activity for hydrogen production [53]. Chen et al. prepared a novel TiO_2-based p–n junction nanotube photocatalyst. The p–n junction nanotube catalyst was shown to have a high photocatalytic activity. We also reported p–n junction photocatalysts p-NiO/n-TiO_2 and p-ZnO/n-TiO_2 [54,55]; the result showed that the photocatalytic reduction activity of p–n junction photocatalyst was higher than that of either n-type semiconductor or p-type semiconductor.

As far as we know, the preparation and properties of p–n junction photocatalyst have not been extensively investigated. It is known that when p-type $CaFe_2O_4$ and n-type ZnO integrate, a p–n junction will be formed between p-$CaFe_2O_4$ and n-ZnO. Theoretically, when p-type $CaFe_2O_4$ and n-type ZnO form p–n junction, the inner electric field will be formed in the interface. At the equilibrium, the inner electric field makes p-type semiconductor $CaFe_2O_4$ region have the negative charge, while ZnO region have the positive charge. Under near UV illumination, electron–hole pairs may be created, and the photogenerated electron–hole pairs are separated by the inner electric field. The holes flow into the negative

* Corresponding author. Tel.: +86 561 3806611; fax: +86 561 3803141.
E-mail address: chshifu@hbcnc.edu.cn (C. Shifu).

1385-8947/$ – see front matter © 2009 Elsevier B.V. All rights reserved.
doi:10.1016/j.cej.2009.07.009

field and the electrons move to the positive field. As a result, the photogenerated electrons and holes are separated efficiently, and the photocatalytic activity is enhanced.

In this study, p-type $CaFe_2O_4$ powder was prepared by the conventional solid state reaction [56]. The p–n junction photocatalyst p-$CaFe_2O_4$/n-ZnO was prepared by ball milling of ZnO in H_2O doped with p-$CaFe_2O_4$. The photocatalyst was characterized by X-ray powder diffraction (XRD), scanning electron microscopy (SEM), transmission electron microscopy (TEM), UV–vis diffuse reflection spectrum (DRS) and fluorescence emission spectra. The photocatalytic activity of the photocatalyst was evaluated by the photocatalytic degradation of methylene blue (MB). Effect of ball milling time on the photocatalytic activity of the photocatalyst was discussed. The possible mechanisms of p–n junction formation and separation of photoexcited electron and hole were also investigated.

2. Experimental

2.1. Materials

The ZnO (wurtzite phase, with crystallite size of about 20 nm), methylene blue (MB), iron oxide (Fe_2O_3), calcium carbonate ($CaCO_3$) and other chemicals used in the experiments are of analytically pure grade. They were purchased from Shanghai and other China Chemical Reagent Ltd. without further purification. Deionized water was used throughout this study.

2.2. Preparation of p-$CaFe_2O_4$ powder

p-Type $CaFe_2O_4$ powders were prepared by the conventional solid state reaction [56]. Fe_2O_3 and $CaCO_3$ were used as the starting materials. These powders were mixed and then heat treated at temperature 1100 °C for 2 h. The synthesized p-type $CaFe_2O_4$ powders were ground in the agate ball milling tank. The powders were wine in color under the preparation conditions.

The mixture transforms to mainly calcium ferrites ($CaFe_2O_4$) according to following equations:

$$CaCO_3 = CaO + CO_2 \quad (1)$$

$$CaO + Fe_2O_3 = CaFe_2O_4 \quad (2)$$

XRD results showed when the heat treatment temperature is 1100 °C, the crystal phase is completely transformed into the $CaFe_2O_4$ phase without any impurity component.

2.3. Preparation of p–n junction photocatalyst p-$CaFe_2O_4$/n-ZnO

The preparation of p-$CaFe_2O_4$/n-ZnO_2 photocatalyst was carried out in a QM-1F ball miller (made in Nanjing University). The procedures are as follows: ZnO powder and agate balls were mixed in the agate ball milling tank in a ratio of 1:10, and then a certain amount of p-$CaFe_2O_4$ (0–10 wt.%) and H_2O were added. After milling for a certain time (0–24 h) at a speed of 700 revolutions per minute (rpm), the wet powder was dried at a temperature of 110 °C in air. The final samples were used for the determination of photocatalytic activity and characterization.

2.4. Photoreactor and procedure

Experiments were carried out in a photoreaction apparatus. The schematic diagram is shown in Fig. 1. The apparatus consists of two parts. The first part is an annular quartz tube. A 375 W medium pressure mercury lamp (Institute of Electric Light Source, Beijing) with a maximum emission at about 365 nm is laid in the empty chamber of the annular quartz tube, and running water passes through an inner thimble of the annular tube. Owing to continuous cooling, the temperature of the reaction solution is maintained at approximately 30 °C. The second part is an unsealed beaker of a diameter 12 cm. At the start of the experiment, the reaction solution (volume, 300 cm^3) containing reactants and photocatalyst was put in the unsealed beakers, and a magneton was used to stir the reaction solution. The distance between the light source and the surface of the reaction solution is 11 cm. The UV irradiation intensity of the reaction solution surface is about 18,300 $\mu W/cm^2$. In the experiment, the initial pH of the reaction solution was about 5.0. The amount of photocatalyst used was 2.0 g/L; the initial concentration of methylene blue (MB) is 1.0×10^{-4} mol/L. The illumination time of each experiment was 20 min. In order to reach the adsorption–desorption equilibrium on the photocatalyst surface, the suspensions were magnetically stirred for 20 min prior to irradiation. After illumination, the samples (volume of each is 5 cm^3) were taken from the reaction suspension, centrifuged at 7000 rpm for 10 min and filtered through a 0.2 μm Millipore filter to remove the particles. The filtrate was then analyzed. In order to determine the reproducibility of the results, at least duplicated runs were carried out for each condition for averaging the results. The blank test was also carried out by irradiating methylene blue (MB) homogeneous solution without photocatalyst for checking the photo-induced self-sensitized photodegradation.

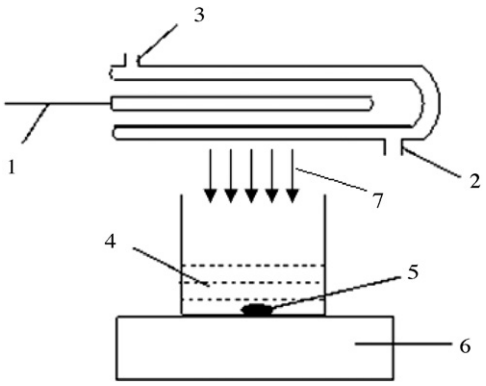

Fig. 1. Schematic diagram of photoreaction apparatus: (1) lamp; (2) water-cooling inlet; (3) water-cooling outlet; (4) reaction solution; (5) stirring rod; (6) magnetic agitator; (7) light.

2.5. Characterization

In order to determine the crystal phase composition and the crystallite size of the photocatalysts, X-ray diffraction (XRD) measurement was carried out at room temperature using a DX-2000 X-ray powder diffractometer with Cu Kα radiation and a scanning speed of 3°/min. The accelerating voltage and emission current were 40 kV and 30 mA, respectively. The crystallite size was calculated by X-ray line broadening analysis using the Scherer equation.

The microcrystalline structure and surface characteristics of the photocatalysts were also investigated by using (X-650 Japan) scanning electron microscopy (SEM).

Transmission electron microscopy (TEM), high-resolution transmission electron microscopy (HR-TEM) images and selected area electron diffraction (SAED) were performed with a JEOL-2010 transmission electron microscope, using an accelerating voltage of 200 kV.

In order to investigate the optical and photochemical properties of the samples, UV–vis diffuse reflectance spectroscopy measurements were carried out using a Hitachi UV-365 Spectrophotometer equipped with an integrating sphere attachment. The analysis range was from 300 to 700 nm, and $BaSO_4$ was used as a reflectance

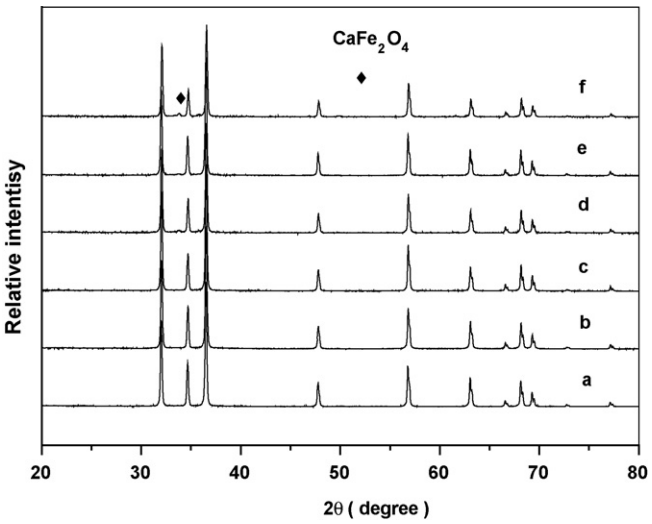

Fig. 2. XRD patterns of photocatalysts: (a) pure ZnO, the amount of doped-p-$CaFe_2O_4$ in the samples of b, c, d, e and f are 0.5 wt.%, 1.0 wt.%, 2.0 wt.%, 5.0 wt.% and 10.0 wt.%, respectively.

standard. Fluorescence emission spectra were recorded on a JASCO FP-6500 type fluorescence spectrophotometer over a wavelength range of 200–730 nm.

2.6. Analysis

The concentration of methylene blue (MB) in solution was determined by spectrophotometer.

The photocatalytic degradation efficiency of methylene blue (MB) was calculated from the following expression:

$$\eta = \frac{C_0 - C_t}{C_0} \times 100\%$$

where η is the photocatalytic efficiency; C_0 is the concentration of reactant before illumination; C_t is the concentration of reactant after illumination time t.

3. Results and discussion

3.1. Characterization of p–n junction photocatalyst p-$CaFe_2O_4$/n-ZnO

3.1.1. XRD analysis

Fig. 2 shows the XRD patterns of photocatalysts ball milled for 6 h. It can be seen that ZnO exhibits dominant diffraction peaks of wurtzite phase. From Fig. 2, it is clear that when the amount of doped p-$CaFe_2O_4$ is lower than 5.0 wt.%, the diffraction peaks of p-$CaFe_2O_4$ cannot be found in XRD patterns. It is proposed that p-$CaFe_2O_4$ may be highly dispersed in the bulk phase of the sample, and the amount of p-$CaFe_2O_4$ is so small that the equipment did not detect its existence. When the amount of doped p-$CaFe_2O_4$ is higher than 5.0 wt.%, the diffraction peaks of p-$CaFe_2O_4$ can be found in XRD patterns. Since no new crystal phases are found, it can be concluded that a new solid is not formed in the ball milling process of ZnO and p-$CaFe_2O_4$.

3.1.2. SEM analysis

SEM was used to investigate the morphology of the samples. The SEM images of p-$CaFe_2O_4$ (1.0 wt.%)/n-ZnO photocatalyst are shown in Fig. 3. It can be seen that the particle shape is spherical, and the mean size of p-$CaFe_2O_4$ (1.0 wt.%)/n-ZnO photocatalyst is about 20–30 nm. The result is the same as that of TEM. From Fig. 3, it also can be seen that when the ball milling time is 24 h, the aggregation degree of the sample is seemingly higher than that of the sample ball milled for 12 h. It agrees with the results of the ball milling time. Namely, when the ball milling time is longer than the optimum time, with the increase in the ball milling time, the fresh surfaces formed by high-energy ball milling possess high surface energy and prefer to agglomerate. In order to determine the aggregation degree of the sample, the experiment of the specific surface area was made. The result showed that when the ball milling time is longer than 12 h, with the increase in the ball milling time, the specific surface area of the sample decreases.

3.1.3. TEM analysis

In order to investigate the interface of the sample, p-$CaFe_2O_4$ (10.0 wt.%)/n-ZnO was chosen for TEM and HR-TEM characterization. Fig. 4a gives an overview of the typical TEM image of the p–n junction photocatalyst p-$CaFe_2O_4$/n-ZnO. It clearly exhibits the existence of ZnO nanoparticles with mean sizes of about 20–30 nm dispersing over the particle of p-$CaFe_2O_4$. Fig. 4b shows the high-resolution TEM (HRTEM) image of the sample. A clear interface can be seen in this figure. The upper part depicts the (1 1 0) plane of ZnO with a spacing of 0.165 nm. The lower part clearly exhibits the $CaFe_2O_4$ (0 2 0) facets with a spacing value of 0.465 nm. The good crystalline quality and the clear interface between ZnO and $CaFe_2O_4$ are advantageous for the separation of the photogenerated charge carriers.

Fig. 5 shows the patterns of the selected area electron diffraction. It can be seen that there are four rings, corresponding to (2 0 3),

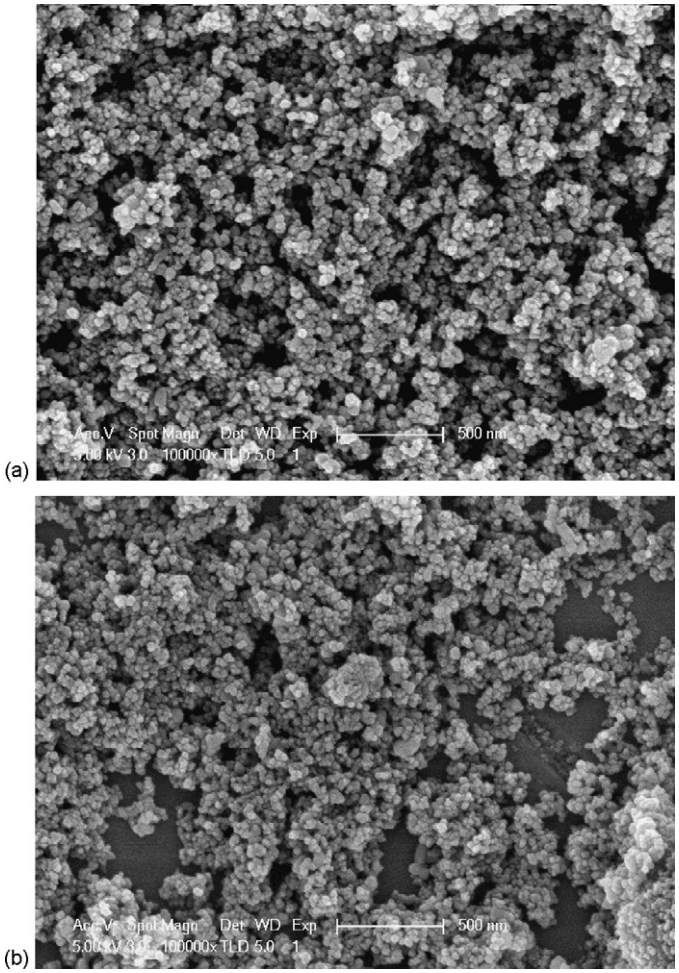

Fig. 3. SEM micrographs of p-$CaFe_2O_4$ (1.0 wt.%)/n-ZnO photocatalyst ball milling time is 12 h and (b) ball milling time is 24 h.

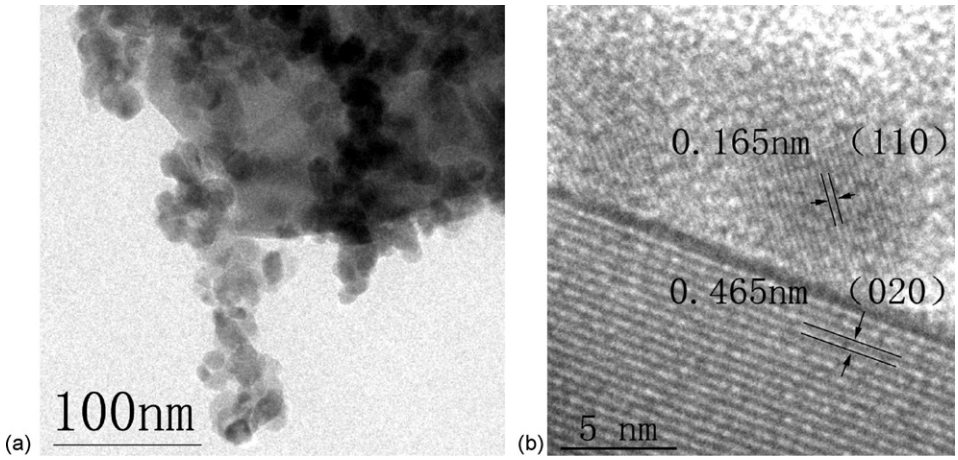

Fig. 4. TEM and HRTEM images of p-$CaFe_2O_4$ (10.0 wt.%)/n-ZnO photocatalyst: (a) TEM image and (b) HRTEM image.

(1 1 0), (1 0 2) and (1 0 3) diffraction planes of the hexagonal structure of ZnO, respectively. Fig. 5b shows the pattern of the selected area electron diffraction of $CaFe_2O_4$. It confirms that the $CaFe_2O_4$ is well crystallized with a single phase orthorhombic structure. Fig. 5c gives an overview of the pattern of the selected area electron diffraction of the p-$CaFe_2O_4$/n-ZnO. It is clear that it consists of the electron diffraction patterns of ZnO and $CaFe_2O_4$. Based on the above results, it is suggested that the p–n junction will be formed by ball milling between ZnO and p-type $CaFe_2O_4$.

3.1.4. UV–vis analysis

Fig. 6 shows UV–vis diffuse reflection spectra of ZnO doped with different contents of p-$CaFe_2O_4$. The samples were ball milled for 6 h. From Fig. 6, it can be seen that the absorption intensity of the photocatalyst is connected with the amount of doped p-$CaFe_2O_4$. The absorption intensity increases with the increase in the amount of doped p-$CaFe_2O_4$. In theory, because the absorption intensity increases, the formation rate of electron–hole pairs on the photocatalyst surface also increases greatly, resulting in the photocatalyst exhibiting higher photocatalytic activity. However, from Fig. 9, it is clear that the photocatalytic activity of p–n junction photocatalyst p-$CaFe_2O_4$/n-ZnO is strongly dependent on the amount of doped p-$CaFe_2O_4$. The photocatalytic activity increases with the increase in the amount of doped p-$CaFe_2O_4$ up to 1.0%. When the amount of doped p-$CaFe_2O_4$ is higher than 1.0%, the photocatalytic activity of the samples decreases. There is no evident relationship between the photocatalytic activity of p-$CaFe_2O_4$/n-ZnO and the absorption intensity. Namely, the high absorption intensity does not increase photocatalytic activity of the photocatalyst in the experimental condition. The similar results were reported in Ref. [57].

Fig. 7 shows UV–vis diffuse reflection spectra of p-$CaFe_2O_4$ (1.0 wt.%)/n-ZnO photocatalyst ball milled for different time. From Fig. 7, it can be seen that with the increase in the ball milling time the absorption wavelength range is extended towards visible light. The reason for the extension of the absorption wavelength range could probably be attributed to the formation of defect energy level in the particles during high-energy ball milling process.

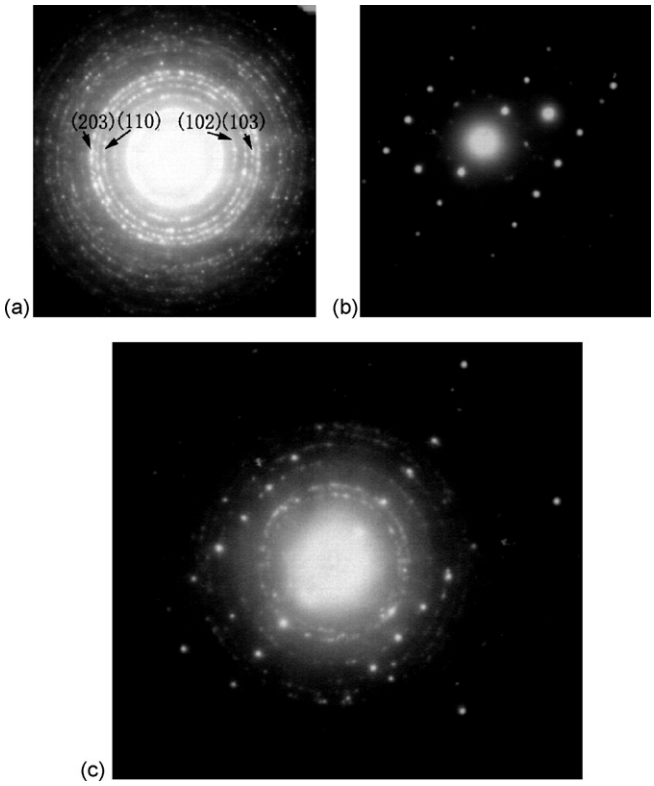

Fig. 5. Selected area electron diffraction pattern: (a) ZnO, (b) $CaFe_2O_4$, and (c) p-$CaFe_2O_4$ (10.0 wt.%)/n-ZnO.

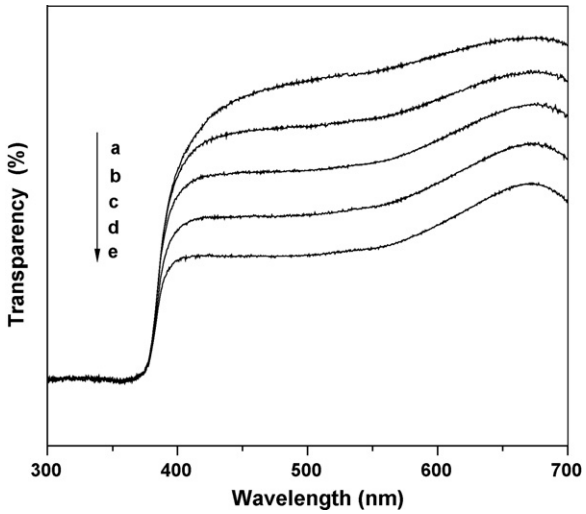

Fig. 6. UV–vis diffuse reflection spectra (a) pure ZnO, the amount of doped-p-$CaFe_2O_4$ in the samples of b, c, d and e are 0.5 wt.%, 1.0 wt.%, 2.0 wt.% and 5.0 wt.%, respectively.

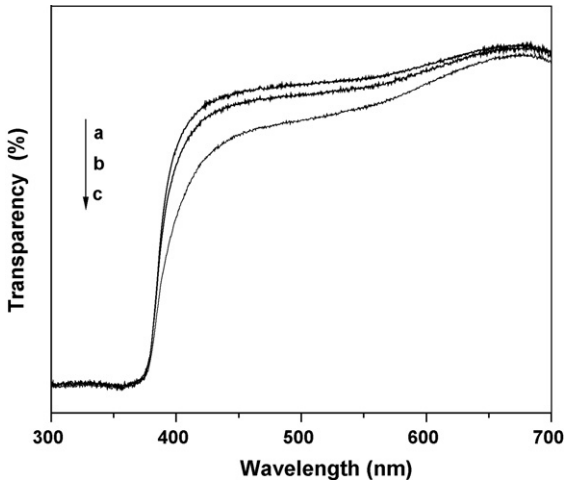

Fig. 7. UV–vis diffuse reflection spectra: (a) ball milling time 3 h, (b) ball milling time 6 h, and (c) ball milling time 12 h.

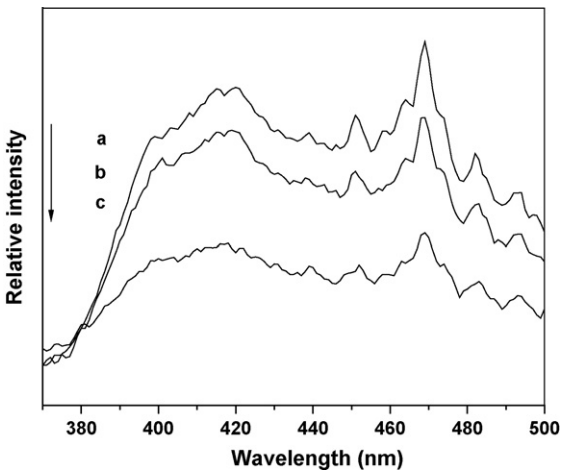

Fig. 8. Fluorescence emission spectra of different samples: (a)ZnO, (b) p-$CaFe_2O_4$ (2.0%)/n-ZnO, and (c) p-$CaFe_2O_4$ (1.0%)/n-ZnO.

In the process of ball milling, the crystal lattices of the $CaFe_2O_4$ and ZnO undergo severe plastic deformation, producing stresses and strains. This creates a crystal lattice distortion, but meanwhile many defects are formed inside particles. These defects have high lattice distortion energy and surface energy. This makes the activation energy for diffusion of elements decrease markedly, and allows for atomic or ionic marked diffusion among elements at room temperature. When the activity of the powder system is high enough, during the ball milling process, the collision between balls and grains of the powder will produce a rise in the interface temperature, which will induce the coupling reaction mentioned here. So, when the interfaces of the $CaFe_2O_4$ and ZnO contact with each other, the p–n junction photocatalyst p-$CaFe_2O_4$/n-ZnO can be formed [34].

3.1.5. Fluorescence emission spectra

Fluorescence emission spectra studies give an insight into the optical and photochemical properties of the samples. Photocatalysts generate electrons and holes after being activated by light, and recombination of some electrons and holes can release energy in the form of fluorescence emission. Lower fluorescence emission intensity implies lower recombination rate of electron–hole [58,59].

Using an ultraviolet light with a 280 nm wavelength as the excitation source, the fluorescence emission spectra of ZnO doped with different contents of p-$CaFe_2O_4$ are shown in Fig. 8. It can be seen that the sample has a strong emission peaks at around 468 nm (2.6 eV). This emission peak corresponds to the blue light due to oxygen vacancy [60]. It is clear that the relative intensity of the emission spectra of ZnO has the greatest relative intensity, which means that electrons and holes of ZnO are easy to recombine. And the relative intensity of p-$CaFe_2O_4$ (1.0 wt.%)/n-ZnO is the lowest. The relative intensity of the p–n junction photocatalyst p-$CaFe_2O_4$/n-ZnO is lower than that of ZnO, showing that doping with p-$CaFe_2O_4$ is helpful to inhibit the recombination of electrons and holes and improve the photocatalytic activity.

The p-$CaFe_2O_4$ content can influence the thickness of the superficial space-charge layer of ZnO. Only when the space-charge layer thickness approximates the penetration depth of light into the solid, can all the photoexcited electron–hole pairs be effectively separated [61]. When the p-$CaFe_2O_4$ content is 1.0%, the relative intensity of emission spectra is the lowest, which shows that 1.0% doping quantity of p-$CaFe_2O_4$ can effectively restrain the recombination of electrons and holes. When the p-$CaFe_2O_4$ content is too small, due to the absence of adequate traps, the recombination rate of electron–hole pairs is high. When the doping quantity is considerably high, the absorption of light and generation of electrons-holes are decreased. These analyses also coincide with the photocatalytic activity of the photocatalysts.

3.2. Evaluation of photocatalytic activity

3.2.1. Effect of amount of doped p-$CaFe_2O_4$ on the photocatalytic activity

The blank test shows photo-induced self-sensitized photodegradation has little influence on the results of experiment. Fig. 9 shows the effects of amount of doped p-$CaFe_2O_4$ on the on the photocatalytic activity of p-$CaFe_2O_4$/n-ZnO. The fixed ball milling time for each sample was 6 h, and fixed illumination time for each experiment was 20 min. It can be seen that the photocatalytic activity of p-$CaFe_2O_4$/n-ZnO increases remarkably with the increase in the amount of doped p-$CaFe_2O_4$ up to 1.0%. The optimum amount of doped p-$CaFe_2O_4$ is 1.0%. When the amount of doped is higher than the optimal amount, the photocatalytic activity of p-$CaFe_2O_4$/n-ZnO decreases gradually as the amount of doped p-$CaFe_2O_4$ increases. The results also show that without p-$CaFe_2O_4$ presence, namely, the pure ZnO powder photocatalyst, its photocatalytic activity is the lowest, and the photocatalytic degradation efficiency is 50.1%. When the amount of doped

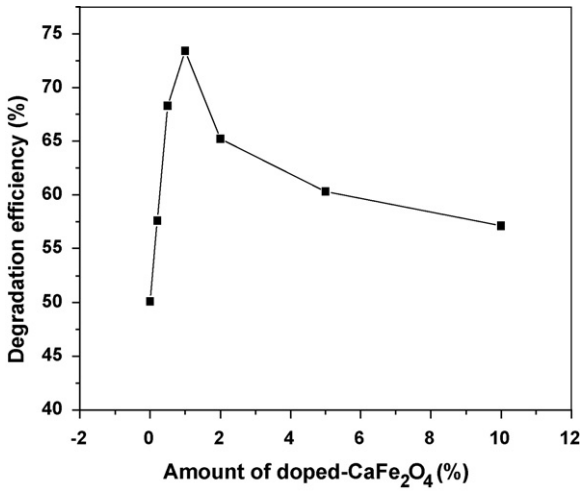

Fig. 9. Effects of amounts of doped p-$CaFe_2O_4$ on the photocatalytic degradation of methylene blue(MB).

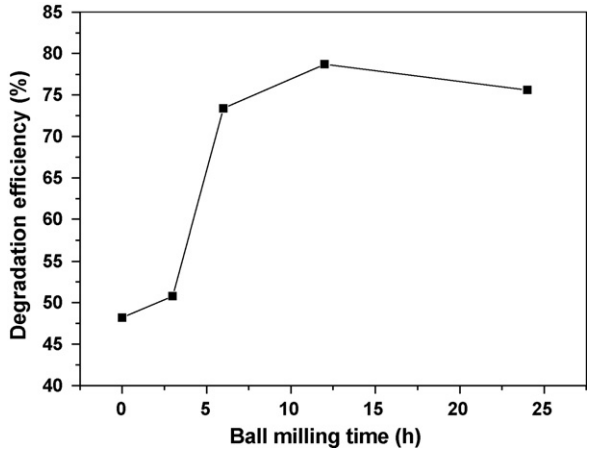

Fig. 10. Effects of ball milling time on the photocatalytic degradation of methylene blue(MB).

p-$CaFe_2O_4$ is 1.0 wt.%, the photocatalytic activity of p–n junction p-$CaFe_2O_4$/n-ZnO photocatalyst is at its peak, and the photodegradation efficiency is 73.4%. It is clear that the photocatalytic activity of p-$CaFe_2O_4$/n-ZnO is higher than that of pure ZnO photocatalyst. It is proposed that, when the amount of p-$CaFe_2O_4$ is lower than its optimum amount of doping, the trapping sites of carriers increase with the increase of the amount of p-$CaFe_2O_4$, which prolongs the lifetime of carriers, thus improving the photocatalytic activity. The other important reason is that the ZnO doped with suitable amount of p-$CaFe_2O_4$, both p-$CaFe_2O_4$ and ZnO can form the p–n junction photocatalyst by ball milling method. Therefore, the photocatalytic activity increases. But when the amount of p-$CaFe_2O_4$ is higher than its optimum amount of doping, the high concentration dopant ions act as recombination centers of electrons and holes, decreases the thickness of the space-charge layer on the photocatalyst particle surface [62].

3.2.2. *Effect of ball milling time on the photocatalytic activity*

The effect of ball milling time on the photocatalytic activity of p-$CaFe_2O_4$ (1.0 wt.%)/n-ZnO photocatalyst is shown in Fig. 10. It can be seen that the ball milling time influences the photocatalytic activity strongly. Without ball milling, the photocatalytic degradation efficiency is 48.2%. The photocatalytic degradation efficiency of methylene blue increases gradually with the increase in ball milling time up to 12 h. When the ball milling time are 3, 6, 12 and 24 h, the photocatalytic degradation efficiencies are 50.8, 73.4, 78.7 and 75.6%, respectively.

The reason is that without ball milling, p-$CaFe_2O_4$ and n-ZnO only play their own photocatalytic role, and the p–n junction photocatalysts are not formed; but after ball milling, p-$CaFe_2O_4$ and n-ZnO can form p–n junction photocatalyst, resulting in the increase of the photocatalytic activity. Another reason is that with the increase in the ball milling time, the specific surface area of the photocatalyst increases. Correspondingly, the number of active sites per unit weight of photocatalyst also increases. But when the ball milling time is longer than the optimum time, it is proposed that with the increase in the ball milling time, the fresh surface formed by high-energy ball milling possess high surface energy and prefer to agglomerate [63].

3.3. *Discussion of mechanism*

It is known that the photocatalytic activity of photocatalyst mainly depends on whether the electron–hole pairs can be separated effectively [64–70]. On the photocatalyst surface, the photoexcited electrons and holes can change in various ways.

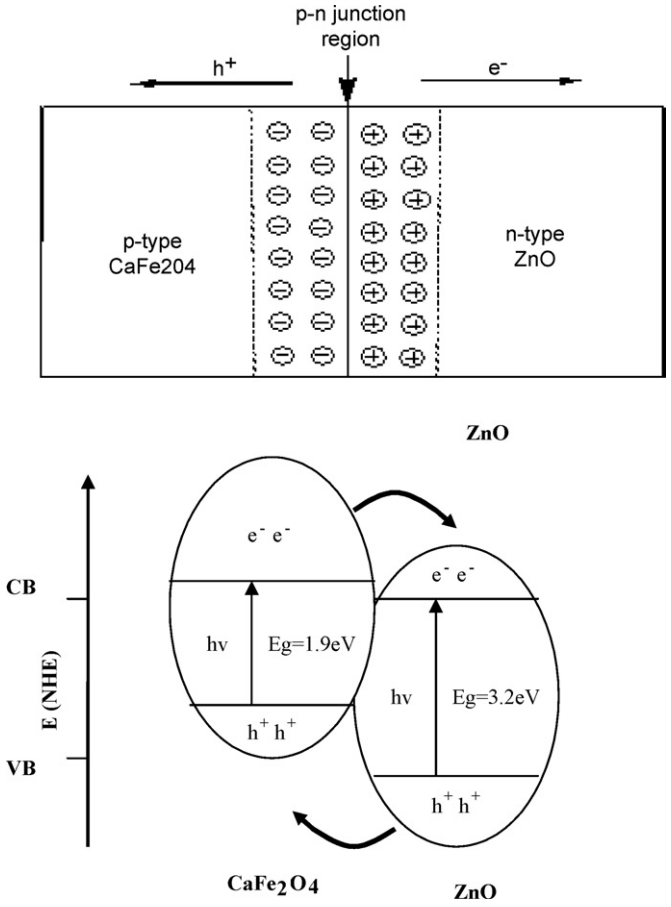

Fig. 11. p–n junction formation model and schematic diagram of photoexcited electron–hole separation process.

Among them, the two competitive processes, i.e., capture and recombination, are the most important ones. Photocatalytic reaction is effective only when the photoexcited electron–holes can be captured. If there are no appropriate capturers of electrons or holes, they will recombine with each other and give off heat inside or on the surface of semiconductor. It is known from the mechanism of separation of electrons and holes that, in order to increase the photocatalytic activity of photocatalyst, two important ways should be considered. One is to increase the separation efficiency of the photoexcited electron–hole pairs, and the other is to increase the amount of the photoexcited activity species [71]. It is known that ZnO is n-type semiconductor, and when doping p-$CaFe_2O_4$ into ZnO granule, a number of micro p–n junction photocatalyst p-$CaFe_2O_4$/n-ZnO will be formed. At the equilibrium, the inner electric field formed which made p-type $CaFe_2O_4$ region have the negative charge while n-type ZnO region have the positive charge. Under near UV illumination, electron–hole pairs may be generated. With the effect of the inner electric field, the holes flow into the negative field while the electrons move to the positive field. Thus, the photogenerated electron–hole pairs will be separated effectively by p–n junction formed in the p-$CaFe_2O_4$/n-ZnO.

Furthermore, according to the band edge position in Fig. 11, as the valence band of p-$CaFe_2O_4$ is lower than that of ZnO [66,72,73], the photoexcited holes on the valence band of the ZnO will transfer to that of the p-$CaFe_2O_4$, and the photoexcited electrons of ZnO will be remained in the conduction band of ZnO. Thus, the photogenerated electron–hole pairs will be separated effectively. The enhancement of photocatalytic performance of p–n junction photocatalyst is attributed to inner electric field assisted charge transfer at

the junction interfaces between the semiconductors with matching band potentials, which consequently favors an effective separation of photoexcited electron–hole in the two semiconductors [74,75]. So the p–n junction photocatalyst p-$CaFe_2O_4$/n-ZnO has higher photocatalytic activity than that of ZnO. According to the above observations, the p–n junction formation model and the schematic diagram of electron–hole separation process are illustrated in Fig. 11.

4. Conclusions

The p–n junction photocatalyst p-$CaFe_2O_4$/n-ZnO was prepared by ball milling method. The photocatalytic activity of p-$CaFe_2O_4$/n-ZnO is higher than that of the pure ZnO. For the photocatalytic degradation of methylene blue (MB), the optimum amount of doped p-$CaFe_2O_4$ is 1.0 wt.%. The ball milling time also influences the photocatalytic activity strongly. With the increase in the ball milling time the absorption wavelength range of p-$CaFe_2O_4$/n-ZnO is extended towards visible light. The optimum ball milling time is 12 h. As the formation of p–n junction photocatalyst p-$CaFe_2O_4$/n-ZnO, the photogenerated electron–hole pairs are separated by the inner electric field, and the photocatalytic activity is enhanced greatly.

Acknowledgements

This work was supported by the Natural Science Foundation of China (No. 20673042), the Natural Science Foundation of Anhui Province (Contract No. 070415211), the Key Project of Science and Technology Research of Ministry of Education of China (208062) and the Natural Science Foundation of Anhui Provincial Education Committee (KJ2007A015).

References

[1] X. Qiu, L. Li, J. Zheng, J. Liu, X. Sun, G. Li, Origin of the enhanced photocatalytic activities of semiconductors: a case study of ZnO doped with Mg^{2+}, J. Phys. Chem. C 112 (2008) 12242–12248.
[2] T. Pauporte, J. Rathousky, Electrodeposited mesoporous ZnO thin films as efficient photocatalysts for the degradation of dye pollutants, J. Phys. Chem. C 111 (2007) 7639–7644.
[3] B. Dindar, S. Icli, Unusual photoreactivity of zinc oxide irradiated by concentrated sunlight, J. Photochem. Photobiol. A: Chem. 140 (2001) 263–268.
[4] M. Mrowetz, E. Selli, Photocatalytic degradation of formic and benzoic acids and hydrogen peroxide evolution in TiO_2 and ZnO water suspensions, J. Photochem. Photobiol. A: Chem. 180 (2006) 15–22.
[5] D. Li, H. Haneda, Morphologies of zinc oxide particles and their effects on photocatalysis, Chemosphere 51 (2003) 129–137.
[6] N. Sobana, M. Swaminathan, The effect of operational parameters on the photocatalytic degradation of acid red 18 by ZnO, Sep. Purif. Technol. 56 (2007) 101–107.
[7] J.G. Yu, X.X. Yu, Hydrothermal synthesis and photocatalytic activity of zinc oxide hollow spheres, Environ. Sci. Technol. 42 (2008) 4902–4907.
[8] C.B. Almquist, P. Biswas, Role of synthesis method and particle size of nanostructured TiO_2 on its photoactivity, J. Catal. 212 (2002) 145–156.
[9] V. Stengl, S. Bakardjieva, J. Subrt, L. Szatmary, Titania aerogel prepared by low temperature supercritical drying, Micropor. Mesopor. Mater. 91 (2006) 1–6.
[10] S. Yoda, D.J. Suh, T. Sato, Adsorption and photocatalytic decomposition of benzene using silica–titania and titania aerogels: effect of supercritical drying, J. Sol–Gel Sci. Technol. 22 (2001) 75–81.
[11] D.M. Antonelli, J.Y. Ying, Synthesis of hexagonally packed mesoporous TiO_2 by a modified sol–gel method, Angew. Chem. Int. 34 (1995) 2014–2017.
[12] F. Bosc, A. Ayral, P.A. Albouy, L. Datas, C. Guizard, Mesostructure of anatase thin films prepared by mesophase templating, Chem. Mater. 16 (2004) 2208–2214.
[13] S. Cao, N. Yao, K.L. Yeung, Synthesis of freestanding silica and titania–silica aerogels with ordered and disordered mesopores, J. Sol–Gel Sci. Technol. 46 (2008) 323–333.
[14] A.J. Maira, W.N. Lau, C.Y. Lee, P.L. Yue, C.K. Chan, K.L. Yeung, Performance of a membrane-catalyst for photocatalytic oxidation of volatile organic compounds, Chem. Eng. Sci. 58 (2003) 959–962.
[15] J. Joo, S.G. Kwon, T. Yu, M. Cho, J. Lee, J. Yoon, T. Hyeon, Large-scale synthesis of TiO_2 nanorods via nonhydrolytic sol–gel ester elimination reaction and their application to photocatalytic inactivation of *E. coli*, J. Phys. Chem. B 109 (2005) 15297–15302.
[16] X. Peng, A. Chen, Aligned TiO_2 nanorod arrays synthesized by oxidizing titanium with acetone, J. Mater. Chem. 14 (2004) 2542–2548.
[17] M. Qamar, C.R. Yoon, H.J. Oh, N.H. Lee, K. Park, D.H. Kim, K.S. Lee, W.J. Lee, S.J. Kim, Preparation and photocatalytic activity of nanotubes obtained from titanium dioxide, Catal. Today 131 (2008) 3–14.
[18] K.L. Yeung, S.T. Yau, A.J. Maira, J.M. Coronado, J. Soria, P.L. Yue, The influence of surface properties on the photocatalytic activity of nanostructured TiO_2, J. Catal. 219 (2003) 107–116.
[19] K.L. Yeung, A.J. Maira, J. Stolz, E. Hung, N.K.C. Ho, A.C. Wei, J. Soria, K.J. Chao, P.L. Yue, Ensemble effects in nanostructured TiO_2 used in the gas-phase photooxidation of trichloroethylene, J. Phys. Chem. B 106 (2002) 4608–4616.
[20] C. Aprile, A. Corma, H. Garcia, Enhancement of the photocatalytic activity of TiO_2 through spatial structuring and particle size control: from subnanometric to submillimetric length scale, Phys. Chem. Chem. Phys. 10 (2008) 769–783.
[21] C.C. Chen, H.J. Fan, J.L. Jan, Degradation pathways and efficiencies of acid blue 1 by photocatalytic reaction with ZnO nanopowder, J. Phys. Chem. C 112 (2008) 11962–11972.
[22] W.Y. Su, Y.F. Zhang, Z.H. Li, L. Wu, X.X. Wang, J.Q. Li, X.Z. Fu, Multivalency iodine doped TiO_2: preparation, characterization, theoretical studies, and visible-light photocatalysis, Langmuir 24 (2008) 3422–3428.
[23] X. Wang, W. Lian, X. Fu, J.M. Basset, F. Lefebvre, Structure, preparation and photocatalytic activity of titanium oxides on MCM-41 surface, J. Catal. 238 (2006) 13–20.
[24] J. Lin, J. Lin, Y.F. Zhu, Controlled synthesis of the $ZnWO_4$ nanostructure and effects on the photocatalytic performance, Inorg. Chem. 46 (2007) 8372–8378.
[25] X. Wang, P. Hu, Y.F. Li, L. Yu, Preparation and characterization of ZnO hollow spheres and ZnO–carbon composite materials using colloidal carbon spheres as templates, J. Phys. Chem. C 111 (2007) 6706–6712.
[26] X.Q. Qiu, L.P. Li, X.Z. Fu, G.S. Li, Size-induced variations in lattice dimension, photoluminescence, and photocatalytic activity of ZnO nanorods, J. Nanosci. Nanotechnol. 8 (2008) 1301–1306.
[27] Y. Zheng, C. Chen, Y. Zhan, X. Lin, Q. Zheng, K. Wei, J. Zhu, Photocatalytic activity of Ag/ZnO heterostructure nanocatalyst: correlation between structure and property, J. Phys. Chem. C 112 (2008) 10773–10777.
[28] H. Tang, J.C. Chang, Y. Shan, S.T. Lee, Surfactant-assisted alignment of ZnO nanocrystals to superstructures, J. Phys. Chem. B 112 (2008) 4016–4021.
[29] Z. Wen, G. Wang, W. Lu, Q. Wang, Q. Zhang, J. Li, Enhanced photocatalytic properties of mesoporous SnO_2 induced by low concentration ZnO doping, Cryst. Growth Des. 7 (2007) 1722–1725.
[30] Z.H. Zhang, Y. Yuan, Y.J. Fang, L.H. Liang, H.C. Ding, L.T. Jin, Preparation of photocatalytic nano-ZnO/TiO_2 film and application for determination of chemical oxygen demand, Talanta 73 (2007) 523–528.
[31] R.Y. Hong, S.Z. Zhang, G.Q. Di, H.Z. Li, Y. Zheng, J. Ding, D.G. Wei, Preparation, characterization and application of Fe_3O_4/ZnO core/shell magnetic nanoparticles, Mater. Res. Bull. 43 (2008) 2457–2468.
[32] S. Cao, K.L. Yeung, P.L. Yue, Preparation of freestanding and crack-free titania–silica aerogels and their performance for gas phase, photocatalytic oxidation of VOCs, Appl. Catal. B 68 (2006) 99–108.
[33] S. Cao, K.L. Yeung, J.K.C. Kwan, P.M.T. To, S.C.T. Yu, An investigation of the performance of catalytic aerogel filters, Appl. Catal. B 86 (2009) 127–136.
[34] S.F. Chen, L. Chen, The preparation of coupled SnO_2/TiO_2 photocatalyst by ball milling, Mater. Chem. Phys. 98 (2006) 116–120.
[35] K. Vinodgopal, P.V. Kamat, Enhanced rates of photocatalytic degradation of an azo dye using SnO_2/TiO_2 coupled semiconductor thin films, Environ. Sci. Technol. 29 (1995) 841–845.
[36] K. Tennakone, J. Bandara, Photocatalytic activity of dye-sensitized tin(IV) oxide nanocrystalline particles attached to zinc oxide particles: long distance electron transfer via ballistic transport of electrons across nanocrystallites, Appl. Catal. A: Gen. 208 (2001) 335–341.
[37] X.Z. Li, F.B. Li, C.L. Yang, W.K. Ge, Photocatalytic activity of WO_x–TiO_2 under visible light irradiation, J. Photochem. Photobiol. A: Chem. 141 (2001) 209–217.
[38] T. Arai, M. Yanagida, Y. Konishi, Y. Iwasaki, H. Sugihara, K. Sayama, Efficient complete oxidation of acetaldehyde into CO_2 over $CuBi_2O_4$/WO_3 composite photocatalyst under visible and UV light irradiation, J. Phys. Chem. C 111 (2007) 7574–7577.
[39] B. Pal, M. Sharon, G. Nogami, Preparation and characterization of TiO_2/Fe_2O_3 binary mixed oxides and its photocatalytic properties, Mater. Chem. Phys. 59 (1999) 254–261.
[40] J. Lin, J.C. Yu, An investigation on photocatalytic activities of mixed TiO_2-rare earth oxides for the oxidation of acetone in air, J. Photochem. Photobiol. A: Chem. 116 (1998) 63–67.
[41] G. Marcı', V. Augugliaro, M.J. López-Muñoz, Preparation characterization and activity of polycrystalline ZnO/TiO_2 systems. 1. Surface and bulk characterization, J. Phys. Chem. B 105 (2001) 1026–1032.
[42] G. Marcı', V. Augugliaro, M.J. López-Muñoz, Preparation characterization and photocatalytic activity of polycrystalline ZnO/TiO_2 systems. 2. Surface, bulk characterization, and 4-nitrophenol photodegradation in liquid–solid regime, J. Phys. Chem. B 105 (2001) 1033–1040.
[43] M.L. Zhang, T.C. An, J.M. Fu, Photocatalytic degradation of mixed gaseous carbonyl compounds at low level on adsorptive TiO_2/SiO_2 photocatalyst using a fluidized bed reactor source, Chemosphere 64 (2006) 423–431.
[44] S.J. Liao, D.G. Huang, D.H. Yu, Y.L. Su, G.Q. Yuan, Preparation and characterization of ZnO/TiO_2, SO_4^{2-}/ZnO/TiO_2 photocatalyst and their photocatalysis, J. Photochem. Photobiol. A: Chem. 168 (2004) 7–13.
[45] O. Khaselev, J. Turner, A monolithic photovoltaic-photoelectrochemical device for hydrogen production via water splitting, Science 280 (1998) 425–427.

[46] J.S. Jang, D.W. Hwang, J.S. Lee, CdS–$AgGaS_2$ photocatalytic diodes for hydrogen production from aqueous Na_2S/Na_2SO_3 electrolyte solution under visible light ($\lambda \geq 420$ nm), Catal. Today 120 (2007) 174–181.
[47] N.R. Tacconi, C.R. Chenthamarakshan, K. Rajeshwar, Selenium-modified titanium dioxide photochemical diode/electrolyte junctions: photocatalytic and electrochemical preparation, characterization, and model simulations, J. Phys. Chem. B 109 (2005) 11953–11960.
[48] J. Akikusa, S.U.M. Khan, Photoelectrolysis of water to hydrogen in p-SiC/Pt and p-SiC/n-TiO_2 cells, Int. J. Hydrogen Energy 27 (2002) 863–870.
[49] F.X. Ye, A. Ohmori, C.J. Li, New approach to enhance the photocatalytic activity of plasma sprayed TiO_2 coatings using p–n junctions, Surf. Coat. Technol. 184 (2004) 233–238.
[50] Z.R. Liu, W.B. Guo, D.G. Fu, W.Y. Chen, p–n heterojunction diodes made by assembly of ITO/nano-crystalline TiO_2/polyaniline/ITO, Synth. Met. 156 (2006) 414–416.
[51] J.L. Li, L. Liu, Y. Yu, Y.W. Tang, H.L. Li, F.P. Du, Preparation of highly photocatalytic active nano-size TiO_2–Cu_2O particle composites with a novel electrochemical method, Electrochem. Commun. 6 (2004) 940–943.
[52] J. Bandara, C.M. Divarathne, S.D. Nanayakkara, Fabrication of n–p junction electrodes made of n-type SnO_2 and p-type NiO for control of charge recombination in dye sensitized solar cells, Sol. Energy Mater. Sol. Cells 81 (2004) 429–437.
[53] H.G. Kim, H.B. Pramod, J.S. Lee, Photocatalytic nanodiodes for visible-light photocatalysis, Angew. Chem. Int. Ed. 44 (2005) 4585–4589.
[54] S.F. Chen, S.J. Zhang, W. Liu, W. Zhao, Preparation and activity evaluation of p–n junction photocatalyst NiO/TiO_2, J. Hazard. Mater. 115 (2008) 320–326.
[55] S.F. Chen, W. Zhao, W. Liu, S.J. Zhang, Preparation, characterization and activity evaluation of p–n junction photocatalyst p-ZnO/n-TiO_2, Appl. Surf. Sci. 255 (2008) 2478–2484.
[56] Y. Matsumoto, M. Obata, J. Hombo, Photocatalytic reduction of carbon dioxide on p-type $CaFe_2O_4$ powder, J. Phys. Chem. 98 (1994) 2950–2951.
[57] B. Gao, Y. Ma, Y. Cao, W. Yang, J. Yao, Great enhancement of photocatalytic activity of nitrogen-doped titania by coupling with tungsten oxide, J. Phys. Chem. B 110 (2006) 14391–14397.
[58] T.J. Cai, M. Yue, X.W. Wang, Q. Deng, Preparation, characterization, and photocatalytic performance of $NdPW_{12}O_{40}/TiO_2$ composite catalyst, Chin. J. Catal. 28 (2007) 10–16.
[59] J.W. Tang, Z.G. Zou, J.H. Ye, Photophysical and photocatalytic properties of $AgInW_2O_8$, J. Phys. Chem. B 107 (2003) 14265–14269.
[60] K. Seungmo, S. Kyoungchul, P. Kandasamy, L. Chongmu, Optical and electrical properties of ZnO doped with nitrogen, Phys. Stat. Sol. (b) 12 (2004) 2830–2834.
[61] M.C. Long, W.M. Cai, J. Cai, B.X. Zhou, X.Y. Chai, Y.H. Wu, Efficient photocatalytic degradation of phenol over $Co_3O_4/BiVO_4$ composite under visible light irradiation, J. Phys. Chem. B 110 (2006) 20211–20216.
[62] S.X. Liu, H. Liu, Fundamental and Application of Photocatalysis and Electrophotocatalysis, first ed., Chem. Ind., Beijing, 2005.
[63] J. Wang, S. Yin, M. Komatsu, Preparation and characterization of nitrogen-doped $SrTiO_3$ photocatalyst, J. Photochem. Photobiol. A: Chem. 165 (2004) 149–156.
[64] W. Zhao, W.H. Ma, C.C. Chen, J.C. Zhao, Z.G. Shuai, Efficient degradation of toxic organic pollutants with Ni_2O_3/TiO_2-xBx under visible irradiation, J. Am. Chem. Soc. 126 (2004) 4782–4783.
[65] H.Y. Lin, Y.F. Chen, Y.W. Chen, Water splitting reaction on NiO/$InVO_4$ under visible light irradiation, Int. J. Hydrogen Energy 32 (2007) 86–92.
[66] M. Long, W.M. Cai, H. Kisch, Visible light induced photoelectrochemical properties of n-$BiVO_4$ and n-$BiVO_4$/p-Co_3O_4, J. Phys. Chem. C 112 (2008) 548–554.
[67] J. Zhang, Q. Xu, Z.C. Feng, M.J. Li, C. Li, Importance of the relationship between surface phases and photocatalytic activity of TiO_2, Angew. Chem. Int. Ed. 47 (2008) 1766–1769.
[68] S.F. Chen, G.Y. Cao, The preparation of nitrogen-doped photocatalyst $TiO_{2-x}N_x$ by ball milling, Chem. Phys. Lett. 413 (2005) 404–409.
[69] J.C. Yu, J. Yu, J. Zhao, Enhanced photocatalytic activity of mesoporous and ordinary TiO_2 thin films by sulfuric acid treatment, Appl. Catal. B: Environ. 36 (2002) 31–43.
[70] D. Dvoranova, V. Brezova, M. Mazur, M.A. Malati, Investigations of metal-doped titanium dioxide photocatalysts, Appl. Catal. B: Environ. 37 (2002) 91–105.
[71] S.F. Chen, L. Chen, The preparation of coupled WO_3/TiO_2 photocatalyst by ball milling, Powder Technol. 160 (2005) 198–202.
[72] L.Q. Jing, B.F. Xin, F.L. Yang, L.P. Xue, B.Q. Wang, H.G. Fu, Effects of surface oxygen vacancies on photophysical and photochemical processes of Zn-doped TiO_2 nanoparticles and their relationship, J. Phys. Chem. B 110 (2006) 17860–17865.
[73] D. Li, H. Haneda, Synthesis of nitrogen-containing ZnO powders by spray pyrolysis and their visible-light photocatalysis in gas-phase acetaldehyde decomposition, J. Photochem. Photobiol. A: Chem. 155 (2003) 171–178.
[74] X.P. Lin, J.C. Xing, W.D. Wang, Z.C. Shan, F.F. Xu, F.Q. Huang, Photocatalytic activities of heterojunction semiconductors $Bi_2O_3/BaTiO_3$: a strategy for the design of efficient combined photocatalysts, J. Phys. Chem. C 111 (2007) 18288–18293.
[75] X.P. Lin, F.Q. Huang, J.C. Xing, W.D. Wang, F.F. Xu, Heterojunction semiconductor $SnO_2/SrNb_2O_6$ with an enhanced photocatalytic activity: the significance of chemically bonded interface, Acta Mater. 56 (2008) 2699–2705.